### 1

# **Energy Conversion in Ni-Mn-Ga with Asymmetrical Bias Magnetic Field**

Medha Veligatla, Paul Lindquist, Carlos J. Garcia-Cervera and Peter Müllner

Abstract—We studied the mechano-electric energy conversion for Ni-Mn-Ga alloys with dynamic experiments under a bias magnetic field. At low and at high magnetic fields, the magneto-crystalline anisotropy energy and the Zeeman energy dominate the formation of magnetic domains. At lower fields and when the bias field is tilted against the twin boundary, the formation of 180° magnetic domains reduces the net magnetization parallel to the load axis. However, at low strains and in a compressed state and when the bias field is tilted along the twin boundary, the majority of the volume saturates parallel to the load axis. Therefore, due to increased net magnetization parallel to the load axis, the magnetic structure generated at lower bias fields tilted parallel to the twin boundary is more favorable to maximize power conversion. However, from experiments, we find that the minimum bias field required to expand the sample against the axial load must be higher than the switching field. Therefore, in order to optimize electric power output, the energy conversion has to take place at lower bias magnetic fields and on samples with low twinning stress with the field direction inclined nearly parallel to the twin boundaries.

*Index Terms*— Mechano-electric energy, Power harvesting, Magnetic shape memory alloys, Ni-Mn-Ga

### I. INTRODUCTION

Magnetic shape memory (MSM) alloys are classified as a group of functional materials that exhibit large recoverable strains. Depending on the martensite structure these materials exhibit magnetic field induced strains up to 12% strain [1]–[4]. The strain in these materials is due to the crystallographic reorientation that occurs via twinning [5]. Due to the magneto-crystalline anisotropy, the magnetization in the sample changes with the movement of the twin boundary [6], [7], and thus does the magnetic flux. The reverse phenomenon, i.e. deformation-induced change of magnetization, is called the inverse magneto-plastic (IMP) effect [8]. When an MSM alloy is subjected to a cyclic mechanical load in the presence of a bias magnetic field that is perpendicular to the load axis, the sample undergoes compression while loading and elongation while unloading. During the cyclic loading and unloading, the sample undergoes a cyclic magnetic flux variation due twin boundary movement (occurring due to continuous sample elongation and compression). When the sample is placed inside a conductive coil, the cyclic load induces an AC voltage

We acknowledge high-performance computing support of the R2 compute cluster (DOI: 10.18122/B2S41H) provided by Boise State University's Research Computing Department. This research was supported in part by the National Science Foundation under project number DMR-1710640.

M. Veligatla was with the Micron School of Materials Science and Engineering, Boise State University, ID 83725 USA (e-mail: medha.veligatla@gmail.com).

P. Lindquist is with Micron School of Materials Science and Engineering, Boise State University, ID, 83725, USA and visiting scientist at Institute of Physics of the Czech Academy of Science (e-mail: paullindquist@boisestate.edu).

C. J. Garcia-Cervera is with University of California, Santa Barbara CA 93106 USA and Visiting Professor at BCAM – Basque Center for Applied Mathematics, Basque Country, Spain

P. Müllner is with Micron School of Materials Science and Engineering, Boise State University, ID 83725 USA (e-mail: petermullner@boisestate.edu)

[9], [10]. These power harvesting capabilities of MSM alloys under a bias magnetic field applied perpendicular to the loading direction were reported by various research groups [9], [11]–[15]. The voltage output generation depends on various experimental factors such as the sample size, the number of turns in the conductive coil, the stroke length, the frequency of cycling, the biased magnetic field and also the direction of the biased field.

Nelson et *al.* [16] conducted initial experiments and also developed a model to characterize the power harvesting capability of MSM alloy by tilting the sample in a transverse magnetic field. Recently Guiel et. *al.* [17] showed that the voltage output can be maximized when the bias field was applied 10-20° (or 100-110° in the present study) to the loading direction. For a sample size of 20 x 3 x 3 mm³, the maximum voltage output obtained was 1280 mV (peak-to-peak voltage) at 9.34° away from the transverse direction and along the twin boundary (corresponding to 99.34° in the present study) with transverse (inclined) and axial magnetic fields. This was a 10-fold increase over the output voltage of 122 mV when the bias magnetic field was applied perpendicular to the loading axis. Guiel *et al.* used finite elemental analysis to study the internal magnetic flux density of MSM alloys and concluded that the dramatic increase in voltage output with magnetic field direction change is due to the internal magnetic structure, albeit without detailing the nature of that structure.

In the present study, through experiments we investigated the voltage/power generation capabilities of an MSM alloy with a sample size of 7.54 x 3.54 x 2.04 mm<sup>3</sup>. We also used micromagnetics to study the evolution of domain structures as a function of magnetic field inclination away from perpendicular to the load axis. From the results obtained with experiments and numerical calculations, we evaluate the influence of magneto-crystalline anisotropy and Zeeman energy on the internal magnetization orientation. We show that the asymmetrical behavior of energy harvesting capability with inclined magnetic field at lower magnetic fields is due to strong magneto-crystalline anisotropy and the formatoin of magnetic domains. Whereas, at higher magnetic fields, the Zeeman energy determines the orientation of magnetization and reduces the energy conversion efficiency.

### II. EXPERIMENTS AND SIMULATIONS:

A single crystal with nominal composition Ni<sub>50.5</sub>Mn<sub>27.75</sub>Ga<sub>21.75</sub> was grown by the Bridgman-Stockbarger technique using the crystal growth system developed by Kellis et *al.*[18]. A sample was cut from the end nearest to the seed that had 10 M crystal structure and a composition of Ni<sub>49.66</sub>Mn<sub>y28.98</sub>Ga<sub>221.36</sub> as determined with energy-dispersive X-ray spectroscopy (EDS). A wire saw was used to cut parallel to {100} faces of the crystal and the sample was polished mechanically with paper and slurry with a final diamond size of 1  $\mu$ m. The final sample shape was 7.54 x 3.54 x 2.04 mm³ when fully extended. The transformation temperatures of the sample were measured at a low magnetic field (250 Oe) in a vibrating sample magnetometer (MicroSense Model 10 VSM) while heating and cooling from 25 °C to 70 °C. The transformation temperatures were  $M_s$  = 41.4 °C,  $M_f$  = 37.8 °C  $A_s$  = 45.5 °C and  $A_f$  = 47.9 °C.

A screw-driven mechanical test system Zwick-1455 (Zwick, Um) was used to obtain the full stress-strain response (0 to 6% strain) of the sample. The sample was fully elongated before the test was performed. The bottom end of the sample was glued to the apparatus and the sample was mechanically loaded under compression with a constant strain rate = 0.125 mm/min. A magnetic field of 0.6 T was applied perpendicular to the load axis during the compression test. The system was equipped with a 500N load cell (MTS, Schaffhausen) and extensometers that are insensitive to magnetic fields (Heidenhain, Traunreut). The resolutions were better than 0.5N in force and 10 nm in displacement. The magnetic field produced by a permanent magnet system (Magnetic Solutions, Dublin) was better than 1% homogeneous at the position of the sample for field strength and field direction. In the test apparatus, the sample was mounted with the longest edge parallel to the mechanical load direction. The magnetic field application was constant and parallel to the shortest edge of the sample.

The Magneto-Mechanical Test Apparatus (MMTA, shown in supporting document, Fig. S1) was used to measure the magneto stress strain measurements, and electrical work in a rotating magnetic field. The MMTA system consists of an electromagnet, a voice coil linear motor, a LVDT displacement transducer, a custom made signal conditioning module scaled to output  $\pm$  300  $\mu$ m displacement, a sample compression micrometer with 1  $\mu$ m sensitivity, a 44 N piezoelectric load cell with  $\pm 15\%$  sensitivity i.e. 112410 mV/kN), interchangeable die springs, and a 1601 turn (inner diameter of 6.2 mm by 11 mm long) 43 AWG pickup coil wound with 0.0031 mm<sup>2</sup> insulated copper wire. The electromotive force, E, induced in the pickup coil was measured with a SR-830 DSM lock-in amplifier (Stanford Research Systems, CA), locked into the displacement voltage signal. When the lock-in amplifier is used in sync mode the instrument outputs the power is computed using the  $V_{rms}$  and the load resistor shunted across the coil, 290  $\Omega$ . The details of this test apparatus, its working and processing of raw data are described in [12]. In this set up, magneto stress strain measurements were obtained at magnetic field ranging from 0.20 to 0.61 T. The magnetic fields were measured from a hall probe with corrected accuracy of ±0.50% to 35 kG (at 25° C) that was centered between the electromagnets such that the flat ends (of the hall probe) are perpendicular to the field direction. In this apparatus, the Ni-Mn-Ga crystal, was centered and glued to one side of the brass platen. The sample was placed such that the long edge was parallel to the load axis. Before testing, the magnetic field on the sample was ramped to about 0.6 T without constraint from the opposite brass platen and the sample expanded to the maximum length. Then the sample was compressed against a set of compliant springs of the actuation system, where the initial displacement was recorded with an in-line micrometer. The compliance of the actuation system accommodated a portion of the displacement such that the initial strain on the sample was different from the displacement. We therefore corrected the initial sample strain such that the first stress-strain loop started at 0% and the last compression loop ended at 6% strain (which is the twinning strain of 10M Ni-Mn-Ga), while the other loops were placed between 0 and 6% with equal intervals. Cyclic stress-strain curves were generated by loading and unloading the sample with a voice coil motor under a magnetic field biased perpendicular to the load axis. We conducted the following test sequence: (1) we obtained stress-strain curves for initial displacements ranging from 0.05 to 0.35 mm at 0.618 T bias magnetic field; (2) we repeated these experiments at magnetic bias field strength of 0.20 T, 0.31 T, 0.39 T, 0.50 T and 0.61 T; (3) we repeated these experiments for frequencies ranging from 50 to 125 Hz; (4) we repeated these experiments for peak-to-peak displacements ranging from 40 μm to 100 μm (stroke length); (5) we repeated these experiments for various directions of the magnetic field ranging from 76 to 104° with respect to the loading axis (i.e. 90° was perpendicular to the loading axis; the field orientation is shown in supporting document, Fig. S2) and varying the peak-to-peak displacements from 40 μm to 180 μm. While doing the cyclic loading and unloading in the MMTA, the sample was placed inside the pickup coil with the coil axis oriented parallel to the mechanical load axis.

Micromagnetic simulations were conducted to obtain the magnetic energies for each equilibrium state in a rotating magnetic field. Magnetic field ranging from 0.1 T to 0.6 T were applied to the sample edge (long axis of the sample). The direction of this magnetic field was varied from 75° to 105° with respect to load axis at 3° intervals (i.e. 90° was perpendicular to the load axis). This study was conducted on samples with strain varied from 1 to 5% strain with 1% increments. Their corresponding sample sizes for 1 and 5% strain are 1.56  $\mu$ m x 0.53  $\mu$ m x 0.36  $\mu$ m and 1.63  $\mu$ m x 0.50  $\mu$ m x 0.36  $\mu$ m respectively. A single twin boundary inclined at 45° to the sample edge was introduced. The position of the twin boundary was determined by the strain on the sample i.e. the fraction  $f_i$  of region with the c-axis (axis of easy magnetization) parallel ( $f_i$ ) and perpendicular ( $f_i = 1 - f_i$ ) to the sample length was determined by the strain  $\varepsilon$  on the sample:  $\varepsilon = f_i$  (1 - c/a), where a and c are the lattice parameters. Therefore the position of the twin boundary changes with the increasing strain on the sample and the c-axis across this twin boundary is nearly perpendicular. The

volume of the simulation sample was divided into 384 cells along the longest dimension and 192 cells along the intermediate dimension making it 73,728 cells in total. Therefore, the dimension of each cell is about 4.06 nm x 2.7 nm (at 1% strain) and each of these cells has one assigned magnetization vector. Each simulation ran for 20,000 iterations. This sequence was repeated with the end configuration serving as input for the new simulation to a total of 180,000 iterations to ensure convergence. Magnetic energies, domain structures and the individual magnetic energy contributions (anisotropy, exchange, and stray field energy) for the equilibrium state were also obtained during these simulations. The simulation code solved the Landau-Lifshitz-Gilbert equation as described in detail in ref. [19].

### III. RESULTS

The stress-strain curve obtained from the static deformation test under a  $0.6~\mathrm{T}$  bias magnetic field is shown as a dotted curve in Fig. 1. At the beginning of the test, the stress increased rapidly until the material yielded, followed by a plateau-like region with very little work hardening. To compare static and dynamic test results, the two data sets were overlaid in Fig. 1, where the data obtained from MMTA is shown in colors (on-line). The dynamic data stem from the experiments performed with a perpendicular (to the load axis) bias magnetic field of  $0.618~\mathrm{T}$ , the loading frequency was 75 Hz, and the peak-to-peak displacement was 170  $\mu$ m. The dynamic curves have about two fold increase in magnetostress compared to the static deformation curve and the slope of the curves also increased due to the increased strain rate.

The dynamical magneto-mechanical experiments yielded the following results:

# A. Varying magnetic field

Fig. 2, shows the voltage (and power) generated as a function of increasing magnetic field. During this test the magnetic field was increased from 0.202 T to 0.618 T while keeping the frequency and the direction of the magnetic field constant. The test sample was strained to 1.85% and then subjected to a cyclic loading and unloading at 75 Hz with a peak-to-peak displacement of 80  $\mu$ m. The The applied magnetic field was at 77° to the loading axis. The results showed that the output voltage (and power) increased with increasing the field obtaining a maximum of 218.1  $\pm$  0.5 mV (or 170  $\pm$  1  $\mu$ W) at 0.502 T. When the field was further increased to 0.618 T, the voltage (or power) values dropped to 194.11  $\pm$ 0.5 mV (135  $\pm$  1  $\mu$ W).

### B. Varying frequency

Fig. 3, shows the voltage (and power) generated as a function of the loading and unloading frequency. The frequency was increased from 50 to 125 Hz with 25 Hz increments while keeping the field constant at 0.618 T and the direction of the field at 77° to the load axis. During this test, the sample was strained to 1.85% and then subjected to a cyclic loading and unloading test with a peak-to-peak displacement of 80  $\mu$ m. The results showed that the output voltage (or power) monotonically increased with increasing the frequency achieving a maximum voltage (or power) of  $421 \pm 0.5$  mV (or  $634 \pm 1$   $\mu$ W) at 125 Hz. These results also agree with results shown by Lindquist et *al.* [12] that the power output increases with increasing frequency.

### C. Varying the direction of magnetic field

For this experiment, the output voltage (and power) was recorded for test samples that were strained to 1.8%, 3.1%, and 3.7%. At each of these strains, the magnetic field and the cyclic loading and unloading frequency was kept constant at 0.618 T and 75 Hz respectively. During these tests, two parameters were varied: 1. magnetic field inclination (with respect to load axis) from  $76^{\circ}$  to  $104^{\circ}$  with  $2^{\circ}$  increments and 2. peak-to-peak displacement from 40 to  $180 \ \mu m$ . Fig. 4, shows the voltage (and power) generated for these test parameters at 1.8% strain. The output voltage (and power) remained constant (about  $130 \ mV$ ) with increasing field inclination angle from  $76^{\circ}$  to  $84^{\circ}$ . From  $86^{\circ}$  to  $98^{\circ}$ , the output voltage linearly decreased

and converged to nearly 0 mV at 98°. Beyond 98° the output voltage increased linearly up to 104°. Similar behavior was obtained for the sample with 3.7 % strain (not shown here) except that there was a drop in the voltage at  $80^{\circ}$  for low peak-to-peak displacement (40 to 60  $\mu$ m) and at  $82^{\circ}$  for higher peak-to-peak displacements (80 to  $180 \mu$ m). For the sample with 3.1% strain (not shown here), the voltage reduced linearly from  $76^{\circ}$  and converged to 0 mV at  $86^{\circ}$  and  $88^{\circ}$ . From  $90^{\circ}$  to  $100^{\circ}$ , the voltage linearly increased with the increasing field inclination angle and beyond  $100^{\circ}$ , the voltage remained constant.

Micromagnetic simulations were performed for a configuration, which replicated the experiments with the goal to calculate the equilibrium magnetic energy (to confirm energy minimization) and the magnetization along the load axis. Except at 0.1 T, at all magnitudes of the magnetic field, the equilibrium energies converged to minimum value. The deviation for 0.1 T was a computational artifact as the energy did not converge to a minimum within 180,000 iterations. Fig. 5, shows the normalized change in magnetization with sample elongation (i.e. the difference of axial magnetization at 1 and 2%, at 1 and 3%, at 1 and 4%, and at 1 and 5%, normalized by the saturation magnetization) obtained at 0.2 T (Fig. 5a) and 0.6 T (Fig. 5b) as a function of increasing bias magnetic field inclinations (from 75° to 105°). In Fig. 5a, the change in magnetization in the direction of the load axis (i.e. parallel to the long axis of the sample) with increasing magnetic bias field inclination (from 75° to 105°) at 0.2 T was asymmetric with respect to 90°. Whereas at higher magnitudes of magnetic field (i.e. at 0.6 T, Fig. 5b), the data was symmetric about 90°. At both lower (0.2 T) and higher (0.6 T) magnetic fields, the change in magnetization increased with increasing strain difference. The maximum change in magnetization was obtained at 0.2 T when the bias magnetic field was inclined to 96° with respect to the load axis.

Fig. 6, shows the equilibrium magnetic domain structures obtained at low bias magnetic fields (i.e. at 0.2 T) for 1% (Fig. 6a) and 5% (Fig. 6b) strain. The arrows in Fig. 6 indicate the direction of magnetization of its respective domains taken in a central area where the magnetization direction was not impacted by the sample surface. All the structures consisted of a single twin boundary inclined at 45° to the long edge of the sample. In Fig. 6a (i.e. at 1% strain), at 84° and 90° bias field inclinations, the region on the left side of the twin boundary formed 180° domains (red and blue regions) and the blue region became more prominent as the field inclination was increased. The region on the right remained as a single domain (yellow, ↑). At 96° inclination, the structure evolved into a single magnetic domain per twin region (blue - left domain and yellow - right domain). In Fig. 6b (i.e. at 5% strain), the magnetic domain structure remained more or less the same with increasing bias field inclination. The structures consisted of 180° domains (blue and red regions) in the left twin region and a single domain (yellow) in the right region. The magnetic domain structures that results in maximum net magnetization parallel to the loading direction were obtained at 96° of field orientation and are highlighted in dashed boxes.

Fig. 7, shows the equilibrium magnetic domain structures at low magnetic field- 0.2 T (Fig. 7a) and at higher magnetic field- 0.6 T (Fig. 7b) for 1% strain obtained at various magnetic bias field inclinations. The arrows in Fig. 7 indicate the direction of magnetization of its respective domains taken in a central area where the magnetization direction was not impacted by the sample surface. All the structures consisted of a single twin boundary inclined at 45° to the long edge of the sample. At 84° and 90° bias field inclinations, the region on the left side of the twin boundary formed 180° domains (red and blue regions) and the blue region became more prominent at higher field orientation. Whereas the region on the right remained as a single domain (yellow, ↑). At 96° inclination, the structure evolved back into a single magnetic domain per twin domain (blue - left domain and yellow - right domain). In Fig. 7a, at low magnetic field (0.2 T), when the magnetic field is aligned at 96° (i.e. the field is aligned more parallel to the twin boundary), the direction of net magnetization in the left twin domain (blue region) is aligned more towards the load axis. Whereas, in Fig. 7b, at higher magnetic field (0.6 T), when the magnetic field is aligned at 96° (i.e. the field is aligned more parallel to the twin boundary), the direction of net magnetization in the left twin domain is aligned

parallel to the field orientation. The average direction of the magnetization deviated in both twin domains markedly from the direction of easy magnetization, i.e. the magnetization was tilted towards the direction of the magnetic field.

### IV. DISCUSSION

The experimental results in Fig. 3 show that the output voltage linearly increases with increasing frequency at 0.6 T. As the frequency increases, the rate of change of magnetization increases proportionally and so does the output voltage (following Faraday's Law). These results measured at a bias magnetic field at 77° agree with the results reported by Lindquist et. al. [12], Karaman et. al. [13], and Sayyaadi et. al. [20] measured in an orthogonal bias magnetic field. Although a maximum voltage output of  $421 \pm 0.5$  mV was obtained in this study at 0.6 T, this could be enhanced by applying a field of only 0.5 T. We show in Fig. 2, that the maximum output voltage was obtained at 0.5 T. With increasing the stroke length, the volume fraction of the crystal re-orientation increases. This implies that the output voltage (and power) increases due to an increase in change of axial magnetization. This is shown in Fig. 4 where the peak-topeak displacement is increased to 180 µm, resulting in voltage output enhancement. Also, in Fig. 4 the output voltage increases when tilting the bias magnetic field in one direction away from orthogonal to the mechanical loading axis. Conversely, the output voltage decreases while tilting the bias magnetic field to the other direction. Guiel et al. [17] reported a similar effect of the magnetic field inclination. In addition, Guiel et al. showed that the output voltage increases when the magnetic field was tilted so as to become more parallel to the twin boundary as opposed to when tilted so as to become more perpendicular to the twin boundary. We did not identify the orientation of the twin boundaries although from comparison of our results with those of Guiel et. al., we conclude that the twin boundaries were closely parallel to 45° (and not parallel to 135°).

Guiel et. *al*. [17] reported an increase in output voltage from about 27 mV to about 270 mV (RMS voltage) by inclining the magnetic field of 0.7 T to 9.34° from the vertical orientation°. In the present study, with a maximum peak-to-peak displacement of 180 µm we increased the voltage output to about 130 mV (RMS voltage) at 6° away from the perpendicular bias field. This difference in voltage and field inclination angle from reported values to this present study can be attributed to sample size and other experimental differences. Guiel et *al*. tested a sample with dimensions 20 x 3 x 3 mm³, which is almost three times longer than the sample of our study and their pick-up coil had 1,000 turns. In addition to the inclined transverse field, they also applied an axial field by placing permanent magnets at the end of the sample. Also, other microstructural aspects such as number of twin boundaries, or the type of twinning may influence the voltage generation.

The numerical simulations show that the change in magnetization parallel to the load axis increases with increasing deformation/strain (Fig. 5) which implies an increase of power output. The change in magnetization parallel to the load axis is higher at lower bias fields (0.2 T for maximum deformation from 1 and 5% strain) and the maximum value was obtained when the field was inclined at 96°. To explain this drastic increase in magnetization, we use the magnetic structures for 1 and 5% at 0.2 T (Fig. 6). When the inclination of the biased field was such as to increase the angle between the magnetic field and the twin boundary (i.e. field angle below 90°), the net magnetization parallel to the load axis decreased through the formation of 180° magnetic domains (i.e. growth of blue region in Fig. 6a). This is because the formation of 180° magnetic domains results in regions with reverse magnetization (blue and red regions in Fig. 6a). However, when the biased field inclination was such that the magnetic field direction was more parallel to the twin boundary (i.e. at field inclination angles larger than 90°), the net magnetization parallel to the load axis increased drastically (blue regions in Fig. 6a). This drastic change in orientation of internal magnetization (nearly parallel to the load axis) was observed at smaller strains (when the sample is compressed i.e. at 1% strain, Fig. 6a). At larger strains (i.e. at 5% strain, Fig. 6b), when the sample is

elongated, the magnetization was less affected by the bias field inclination. The reason for the asymmetry with respect to strain is in the orientation of the axis of easy magnetization in the majority twin domain. At 1% strain, the larger twin region is oriented with the *c*-axis parallel to the mechanical loading axis, which results in a large net axial magnetization if one areal fractions of the red and the blue magnetic domains is larger than the other. In contrast, at 5% strain, the larger twin is oriented with the *c*-axis perpendicular to the loading axis. This results in a small axial magnetization component. When the bias magnetic field is perpendicular to the loading axis (90°), the head-to-tail orientation of magnetic moments at the twin boundary between the yellow and the red magnetic domains is energetically favored against the head-to-head configuration between the yellow and the blue magnetic domains. This biases the balance between the fractions of the red and the blue magnetic domains towards red and causes a net axial magnetization. Tilting the magnetic field towards perpendicular to the twin boundary assists this bias and leads to a slight increase of axial magnetization. When tilting the magnetic field towards more parallel to the twin boundary, that bias must be overcome before the blue domain dominates the twin with the axis of easy magnetization parallel to the loading axis.

At higher fields, the Zeeman energy overpowers the magneto-crystalline anisotropy energy. The direction of magnetization tends to align more effectively away from the direction of easy magnetization and in the direction of the external magnetic field. An example of this is shown in Fig. 7. Due to the influence of the external field, the orientation of magnetization is shifted away from the load axis (or in the direction of the external field), thus reducing the net magnetization in the direction parallel to the load axis (Fig. 7). Also, the magnetization direction in both twins is more parallel than perpendicular to each other. Thus, moving the twin boundary causes a lesser change in axial magnetization. Irrespective of the inclination of magnetic field against or along the twin boundary, the net magnetization along the load axis is reduced. This reduced variation in axial magnetization at higher fields results in lower power output compared to lower magnetic fields. This effect is experimentally verified in Fig. 2 where the voltage generation and power output have a maximum at 0.5 T and decrease at higher magnetic field.

The decrease of voltage generation and power output with the decreasing magnetic field below 0.5 T as determined experimentally (Fig. 2), results most likely from the reduced effectiveness of the bias magnetic field. To expand the sample against the axial load, the magnetic field must be larger than the switching field, i.e. the magnetostress must overcome the twinning stress [6]. The mechanical hysteresis (Fig. 1) shows that the twinning stress is about 1 MPa. This corresponds to a switching field of about 300 mT [21]. Thus, below 300 mT, the magnetic field is not sufficient to restore the deformation completely. Additionally, in a configuration with the magnetization perpendicular to the long axis of a sample, the magnetic switching of twin domains is a sluggish process [22]. Thus, it takes a substantially higher magnetic field to completely restore the deformation. Thus, the finite mobility of twin boundaries causes a reduction of change of axial magnetization with decreasing magnetic field. This reduction causes the reduction of Voltage generation and power output. By its nature, the numerical simulations carried out in this study consider static twin patterns. Thus, these numerical simulations do not capture the effect of twin boundary mobility and do not reflect the decrease of change of axial magnetization with decreasing magnetic field.

# V. CONCLUSIONS

We used experimental results to evaluate the effect of various factors such as magnetic field, loading frequency, stroke length, and bias field inclination angle on mechano-electrical energy conversion for a Ni-Mn-Ga alloy transducer. We show in agreement with literature data that the voltage output (and power) can be increased with increasing the loading frequency, stroke length (peak-to-peak displacement), and by changing the orientation of the bias magnetic field parallel to the twin boundary. The results obtained in a fixed set up where the alignment of the sample was not disturbed, remained consistent and were repeatable. However, by removing the sample from the set up or by realigning, the repeatability was compromised. Therefore, the energy conversion is sensitive to many factors such as the sample size, the positioning of the

sample within the electromagnets, constraints imposed by fixing the sample, the twin microstructure, and the orientation of the twin boundary with respect to the bias magnetic field inclination.

Using the magnetic domain structures from numerical calculations we analyzed the asymmetry of internal magnetization for various bias magnetic field inclination angles at varying magnitudes of the magnetic field. We conclude that the orientation of internal magnetization is dictated by magnetocrystalline anisotropy at lower fields and by the orientation of the external field at higher magnetic fields (i.e. close to or larger than the saturation field). Also, the power output is maximized at lower magnetic fields (such as 0.2 T or lower than saturation field) due to the increased amount of net magnetization parallel to the load axis. However, reducing the bias magnetic field strength is limited by the twinning stress of the sample. Therefore, in order to generate maximum power output, the energy conversion has to take place at lower magnetic fields and on a sample with low twinning stress.

## VI. ACKNOWLEDGEMENTS

We would like to acknowledge high-performance computing support of the R2 compute cluster (DOI: 10.18122/B2S41H) provided by Boise State University's Research Computing Department. This research was supported in part by the National Science Foundation under project number DMR-1710640.

### VII. REFERENCES

- [1] K. Ullakko, J. K. Huang, C. Kantner, R. C. O'Handley, and V. V. Kokorin, "Large magnetic-field-induced strains in Ni2MnGa single crystals," *Appl. Phys. Lett.*, vol. 69, no. 13, pp. 1966–1968, 1996.
- [2] S. J. Murray, M. Marioni, S. M. Allen, R. C. O'Handley, and T. A. Lograsso, "6% magnetic-field-induced strain by twin-boundary motion in ferromagnetic Ni-Mn-Ga," *Appl. Phys. Lett.*, vol. 77, no. 6, pp. 886–888, 2000.
- [3] O. Söderberg, Y. Ge, A. Sozinov, S. P. Hannula, and V. K. Lindroos, "Recent breakthrough development of the magnetic shape memory effect in Ni-Mn-Ga alloys," *Smart Mater. Struct.*, vol. 14, no. 5, 2005.
- [4] A. Sozinov, N. Lanska, A. Soroka, W. Zou, "12% magnetic field-induced strain in Ni-Mn-Gabased non-modulated martensite," *Appl. Phys. Lett.*, vol. 102, pp. 121902 [1-5], 2013.
- [5] J. Tellinen, I. Suorsa, I. Aaltio, and K. Ullakko, "Basic Properties of Magnetic Shape Memory Actuators," 8th Int. Conf. ACTUATOR 2002, June, 2002.
- [6] P. Müllner, V. A. Chernenko, M. Wollgarten, G. Kostorz, "Large cyclic deformation of a Ni-Mn-Ga shape memory alloy induced by magnetic," *J. Appl. Phys.*, vol. 92, no. 11, pp. 6708–6713, 2002.
- [7] L. Straka and O. Heczko, "Magnetic anisotropy in Ni Mn Ga martensites," *J. Appl. Phys.* vol. 93, no. May 2003, pp. 8636–8638, 2003.
- [8] P. Müllner, V. A. Chernenko, G. Kostorz, "Stress-induced twin rearrangement resulting in change of magnetization in a Ni Mn Ga ferromagnetic martensite," *Scripta. Mater.* vol. 49, pp. 129–133, 2003.
- [9] I. Suorsa, J. Tellinen, K. Ullakko, E. Pagounis, "Voltage generation induced by mechanical straining in magnetic shape memory materials," *J. Appl. Phys.*, vol. 95, pp. 8054-8058, 2004.
- [10] D. Carpenter, M. Chemielus, A. Rothenbühler, R. Schneider, P. Müllner, "Application of ferromagnetic shape memory alloys in power generation devices," *Proc. Int. Conf. Maartensitic Transform.* "ICOMAT-08", St. Fe, NM, pp. 365–369, 2008.
- [11] L. Straka, H. H. Hänninen, N. Lanska, A. Sozinov, "Twin interaction and large magnetoelasticity in Ni-Mn-Ga single crystals," *J. Appl. Phys.*, vol. 109, pp. 063504 [1-7], 2011.
- [12] P. Lindquist, T. Hobza, C. Patrick, P. Müllner, Efficiency of Energy Harvesting in Ni Mn Ga

- Shape Memory Alloys," Shap. mem. Superelasticity, vol. 4, pp. 93–101, 2018.
- [13] I. Karaman, B. Basaran, H. E. Karaca, A. I. Karsilayan, Y. I. Chummlyakov, "Energy harvesting using martensite variant reorientation mechanism in a NiMnGa magnetic shape memory alloy," *J. Appl. Phys. Lett.*, vol. 90, pp. 172505 [1–4], 2007.
- [14] N.M. Bruno, C. Ciocanel, H.P. Feigenbaum A. Waldauer, "A theoretical and experimental investigation of power harvesting using the NiMnGa martensite reorientation mechanism," *Smart Mater. Struct.* vol. 21, pp. 094018 [1-12], 2012.
- [15] N. Bruno, C. Ciocanel, H. Feigenbaum, "Electromitive force generation using the dynamic response if Ni<sub>50</sub>Mn<sub>28.5</sub>Ga<sub>21.5</sub> magnetic shape memory alloy," *Conf. Proc. SPIE*, vol. 79781P, 2011.
- [16] I. Nelson, J. Dikes, H. Feigenbaum, and C. Ciocanel, "Numerical predictions versus experimental findings on the power-harvesting output of a NiMnGa alloy," *Behav. Mech. Multifunct. Mater. Compos. 2014*, vol. 9058, no. March 2014, 2014.
- [17] R. Guiel, H. Feigenbaum, and C. Ciocanel, "The effect of magnetic fi eld orientation on the open-circuit voltage of Ni Mn Ga based power harvesters," *Smart Mater. Struct.*, vol. 27, pp. 095006 [1–15], 2018.
- [18] D. Kellis, A. Smith, K. Ullakko, P. Müllner, "Oriented single crystals of Ni Mn Ga with very low switching field," *J. Cryst. Growth*, vol. 359, pp. 64–68, 2012.
- [19] A. Hobza, C. J. García-Cervera, and P. Müllner, "Twin-enhanced magnetic torque," *J. Magn. Magn. Mater.*, vol. 458, pp. 183–192, 2018.
- [20] H. Sayyaadi and M. A. A. Farsangi, "Frequency-dependent energy harvesting via magnetic shape memory alloys," *Smart Mater. Struct.*, vol. 24, no. 11, 2015.
- [21] V. A. Chernenko, V. A. L'vov, P. Müllner, G. Kostorz, T. Takagi, "Magnetic-field-induced superelasticity of ferromagnetic thermoelastic martensites: Experiment and modeling," *Phys. Rev. B*, vol. 69, pp. 134410 [1–8], 2004.
- [22] M. Veligatla, C. Titsch, W.G. Drossel, C. J. Garcia-Cervera and P. Müllner, "Sensitivity of twin boundary movement to sample shape in Ni-Mn-Ga," *Acta. Mater.*, vol. 186, pp. 389-395 2020.

# **Figures**

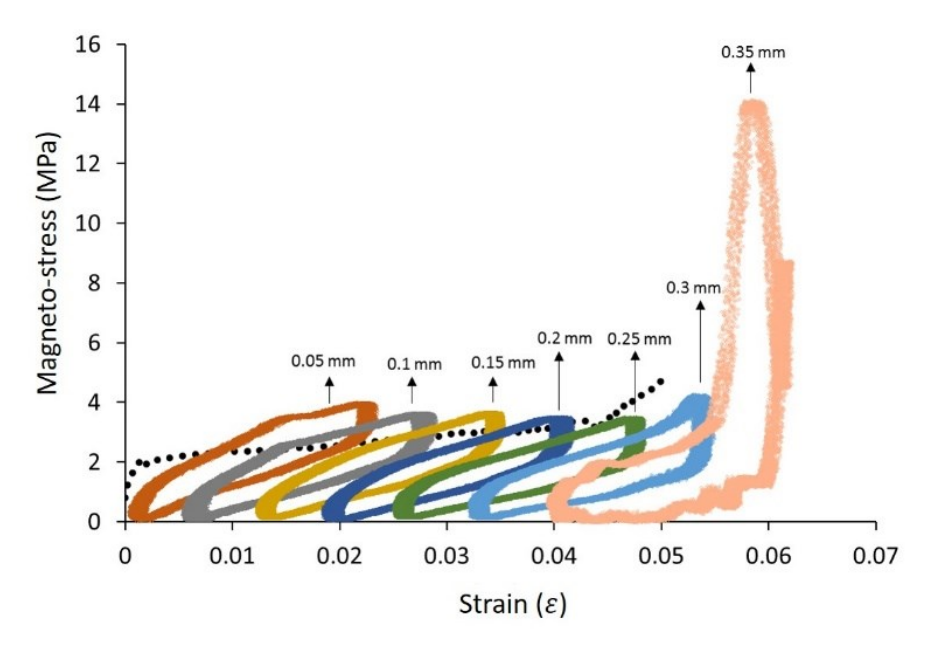


Fig. 1. Stress-strain curves obtained with static and dynamic loading. The static loading under uniaxial compression obtained at a constant strain rate of 125 mm/min and under a perpendicular bias magnetic field of 0.6 T is represented by the dotted line. The dynamical stress-strain loops (color online) were obtained by cyclic loading and unloading at 75 Hz frequency to a peak-to-peak displacement of 170  $\mu$ m. Each stress-strain loop obtained at fixed initial displacements ranging from 0.05 to 0.35 mm with 0.05 intervals at 0.6 T bias magnetic field.

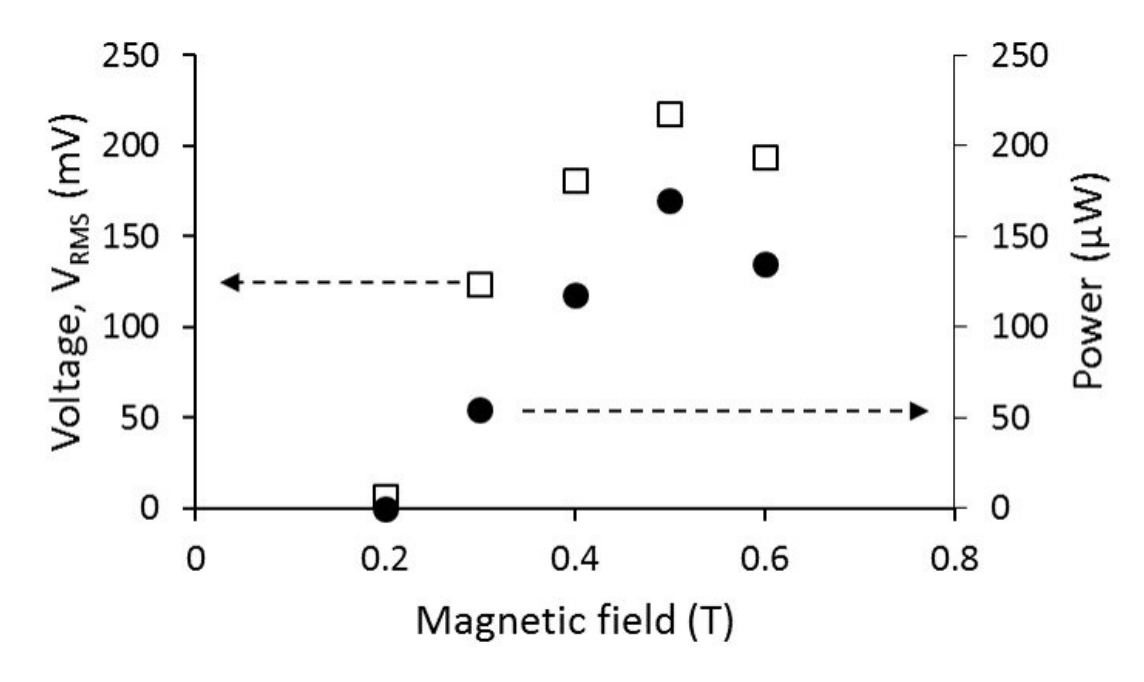


Fig. 2. Voltage,  $V_{RMS}$  (squares) and power output (circles) measured for increasing magnetic field from 0.20 to 0.61 T while keeping the following variables constant at: peak-to-peak displacement 80  $\mu$ m, frequency 75 Hz, bias magnetic field at 77°, and compression on sample 1.8%.

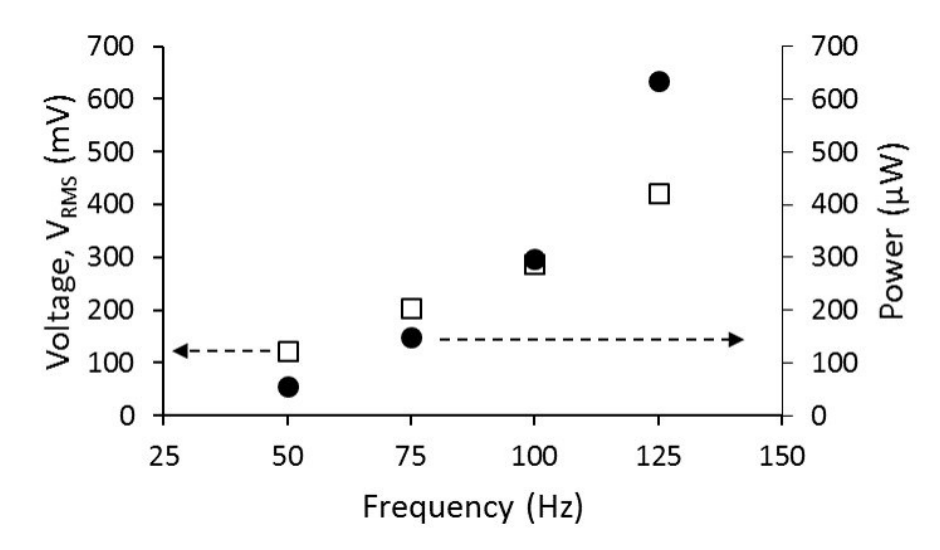


Fig. 3. Voltage (squares) and power output (circles) measured for increasing frequency from 50 to 125 Hz while keeping the following variables constant at: peak-to-peak displacement  $80~\mu m$ , magnetic field 0.61 T, magnetic bias field at  $77^{\circ}$ , and compression on sample 1.8%.

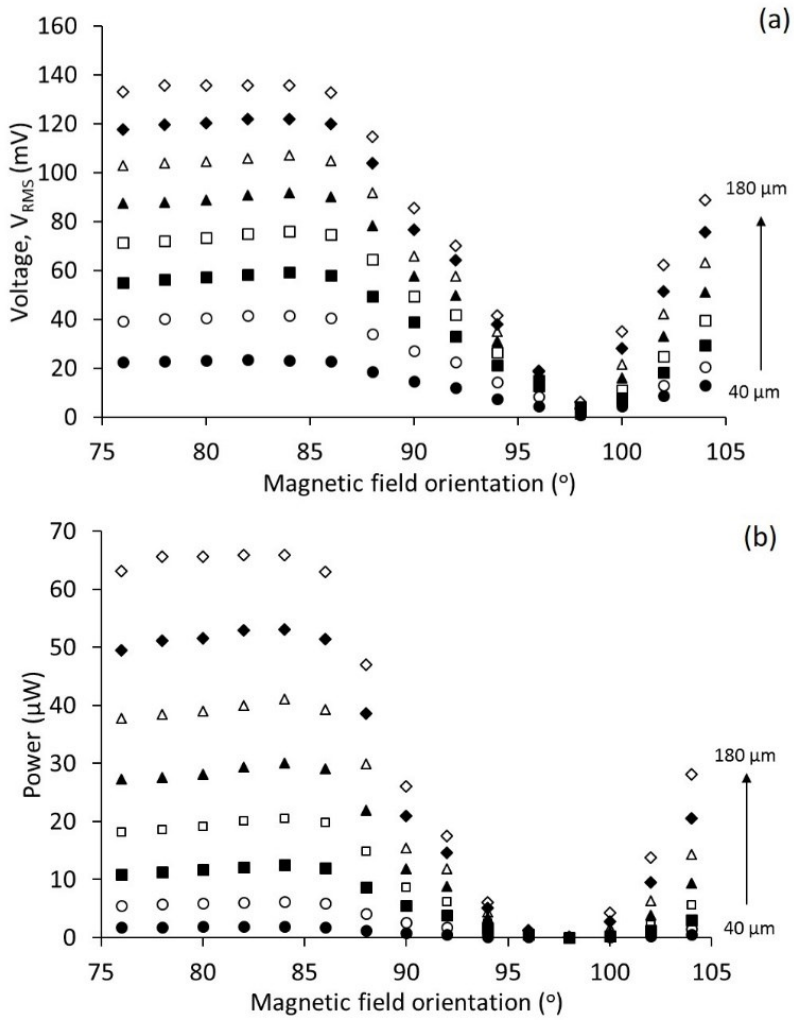


Fig. 4. (a) Voltage output and (b) Power output measured for magnetic bias field orientations ranging from  $76^{\circ}$  to  $104^{\circ}$  with  $2^{\circ}$  interval and peak-to -peak displacements ranging from 40 to  $180~\mu m$  with  $20~\mu m$  intervals. During this experiment, the following variables were kept constant at: magnetic field 0.61~T, frequency 75~Hz, and compression on sample 1.8%.

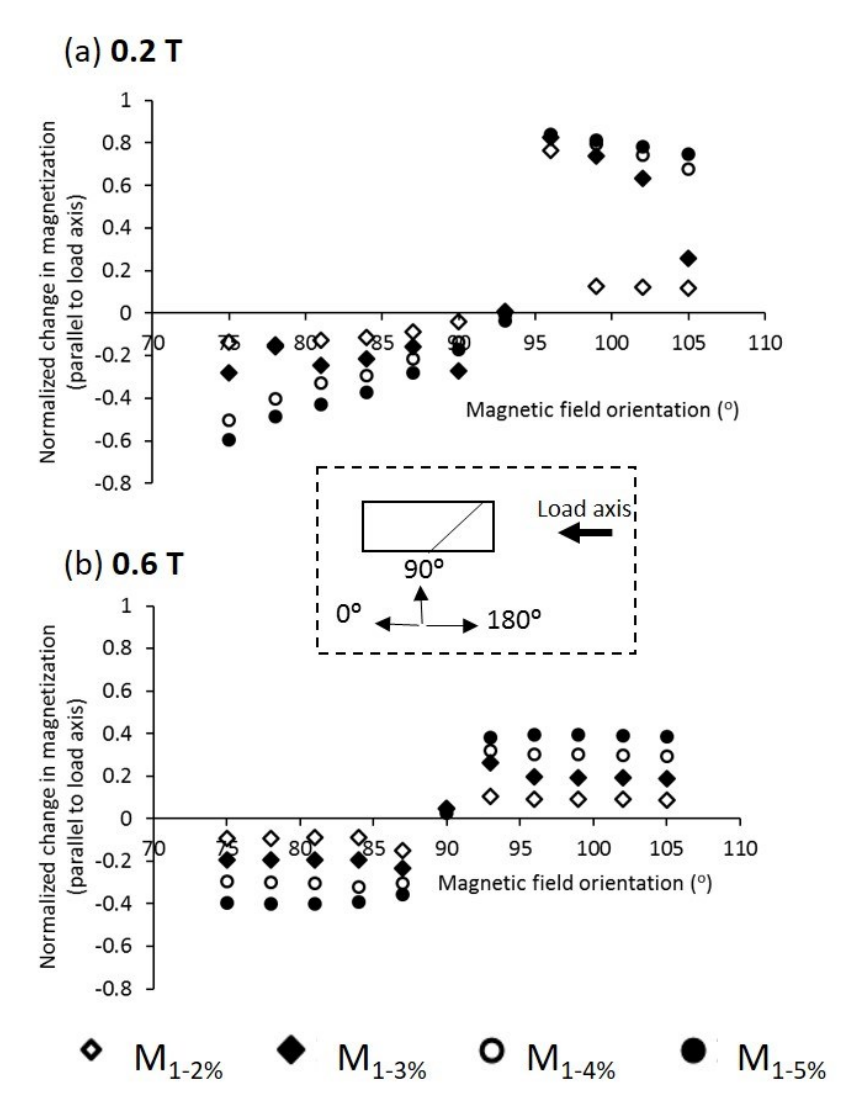


Fig. 5. Normalized change in magnetization along the load axis at various bias magnetic field inclinations (orientations) from 75° to 105° (with respect to load axis) obtained from numerical calculations. The change in magnetization was obtained for (a) 0.2 T and (b) 0.6 T. The inset in between the (a) and (b) is a guide to the field inclination angles and the direction of the load axis with respect to the sample length and inclination of the twin boundary.

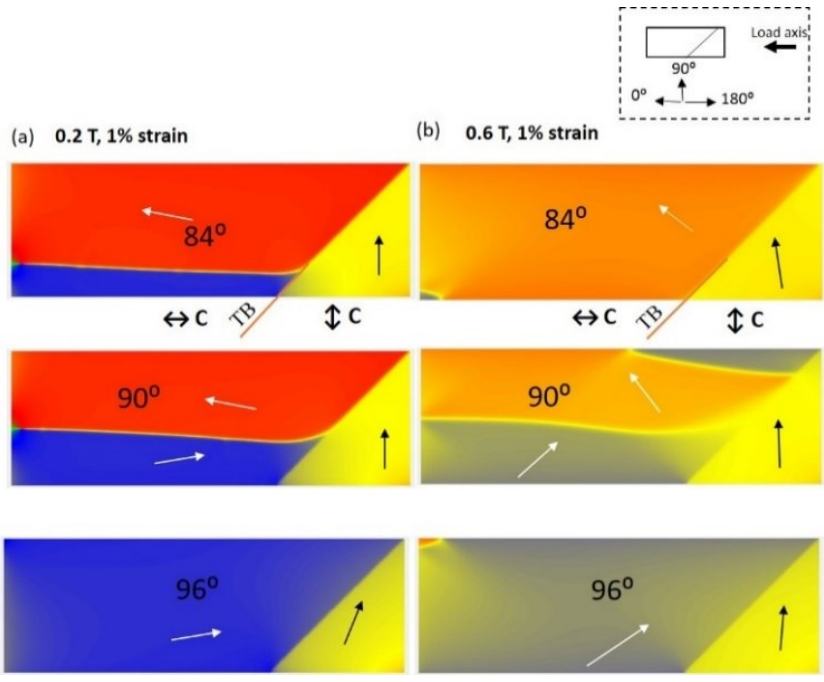


Fig. 6. Shows the comparison of magnetic domain structures at 1% and 5% strain at the low bias magnetic field. Magnetic domain structures were obtained from simulations at (a) 0.2 T, 1% strain and (b) 0.2 T, 5% strain for magnetic bias field orientations at 84°, 90°, and 96°. The orientation of the bias field (with respect to the load axis) is denoted by the numbers on its corresponding domain structures and the direction of magnetization occupied in the center of each magnetic domain is indicated by the arrows. The domain structures that result in maximum net magnetization along the load axis are highlighted in dashed boxes. "TB" denotes twin boundary and "c" denotes the direction of easy magnetization. The schematic on top right is a representation of the sample and the direction of the load axis. The magnetic domain structures corresponding to all magnetic field orientations ranging from 75° to 105° are in supporting document, Fig. S3.

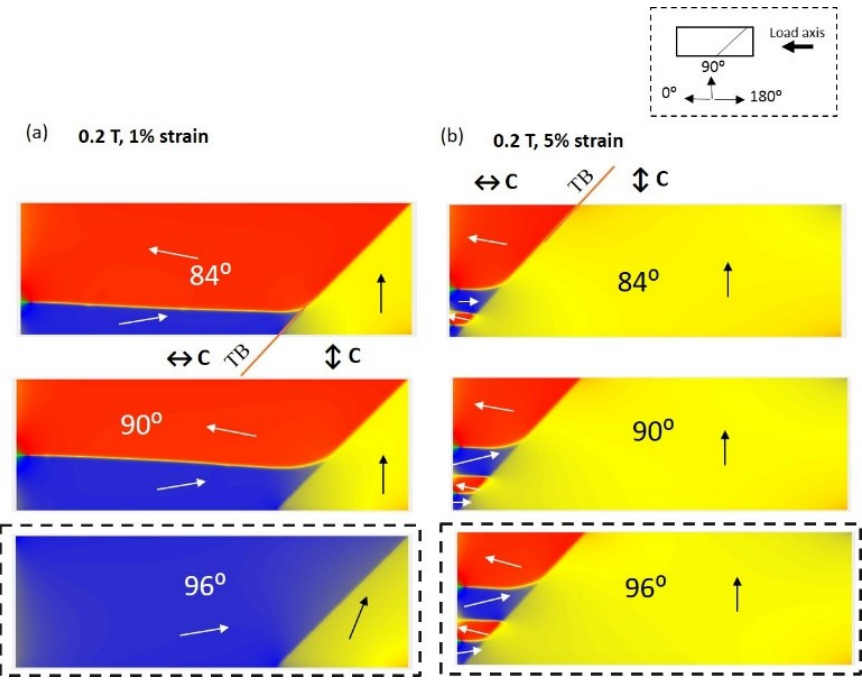


Fig. 7. Shows the comparison of magnetic domain structures at the low and the high bias magnetic fields. Magnetic domain structures were obtained from simulations at (a) 0.2 T, 1% strain and (b) 0.6 T, 1% strain for magnetic bias field orientations at 84°, 90°, and 96°. The orientation of the bias field (with respect to the load axis) is denoted by the numbers on its corresponding domain structures and the direction of magnetization occupied in the center of each magnetic domain is indicated by the arrows. "TB" denotes twin boundary and "c" denotes the direction of easy magnetization. The schematic on top right is a representation of the sample and the direction of the load axis. The magnetic domain structures corresponding to all magnetic field orientations ranging from 75° to 105° in supporting document, Fig. S3.